Electronic Supplementary Material (ESI) for ChemComm.

Supporting Information

Laser Synthesis of Oxygen Vacancy-Modified CoOOH for Highly Efficient Oxygen Evolution

Chao Meng [a], Mengchang Lin [a], Xuechun Sun [b], Xiaodong Chen [a], Xuemin Chen [c], Xiwen Du [b]*, and Yue Zhou [a]*

[a] College of Electrical Engineering and Automation, Shandong University of Science and Technology, Qingdao, 266590, China

[b] Institute of New-Energy Materials, School of Materials Science and Engineering, Tianjin University, Tianjin, 300072, China

[c] College of Science, Hebei University of Science & Technology, Shijiazhuang, 050018, China

* E-mail for Y.Z.: zhouyue@sdust.edu.cn

* E-mail for X.W.D.: xwdu@tju.edu.cn

Experimental Section

Materials: Cobalt target (Co, 99.9 % in purity) was ordered from Beijing Trillion Metals Co., Ltd. Cobalt nitrate hexahydrate ($Co(NO_3)_2\cdot 9H_2O$, 98 % in purity) and ruthenium oxides (RuO_2, 99 % in purity) were purchased from J&K Chemical. Potassium hydroxide (KOH, 98 % in purity) and H_2O_2 solution (30 wt.%) were obtained from Tianjin Jiangtian Chemical Technology Co., Ltd.

Synthesis of B-CoOOH: B-CoOOH nanosheets were synthesized as reported in literature.[1] 0.75 mmol $Co(NO_3)_2\cdot 9H_2O$ was dissolved in the mixed solution of 20 mL ethanol and 10 mL 30 wt.% H_2O_2 solution. Then the solution was transferred into a 50 mL Teflon-lined stainless-steel autoclave and kept at 140 ℃ for 12 h in an oven. After the autoclave cooled down to room temperature, the products were collected and washed with deionized water for several times, and finally freeze-dried for 1 day.

Synthesis of L-CoOOH: L-CoOOH nanosheets were synthesized by 1064 nm laser ablation method. A nanosecond pulsed Nd: YAG laser (Nimma-600 from Beamtech) with pulse width of 7 ns and power density of 6×10^7 W cm^{-2} was applied for sample preparation. Firstly, a pure Co target was polished and washed with distilled water for several times. Afterwards, the Co target was irradiated by nanosecond laser in 1 M KOH at room temperature for 20 min until the solution turns into a brown colloid. Finally, the laser products were collected and washed with deionized water for several times, and then freeze-dried for 1 day.

The R-CoOOH nanosheets were synthesized by the same method, but the power density of laser irradiation was reduced to 4×10^7 W cm^{-2}.

Characterization: The morphologies of prepared CoOOH catalysts were characterized by TEM, HRTEM (JEOL 2100, 200 kV, equipped with EDS), and SEM (FEI Nova NanoSEM 450). XRD patterns were obtained by powder X-ray diffractometer (Siemens-Bruker D5000 XRD). The XPS analyses were collected on a Thermo fisher spectrometer (k-alpha). EPR spectra were obtained by Bruker E500 spectrometer at 25 ℃. AFM was acquired on Veeco DI Nano-scope MultiMode V system.

Electrocatalytic Measurements: The electrochemical measurements were studied with a three-electrode system in 1 M KOH using an electrochemical workstation (CHI-660D, Inc., Shanghai). A platinum sheet and a saturated calomel electrode (SCE) were employed as the counter and the reference electrode, respectively. The working electrode was prepared by dropping catalysts ink on glassy carbon electrode (GCE) with the loading mass of 0.2 mg cm^{-2}. All LSV curves were conducted at a scan rate of 5 mV s^{-1} with *iR*-correction. EIS measurements were performed by applying an ac voltage with 5 mV amplitude within the frequency range of 0.05 to 200 kHz.

1. Characterizations of CoOOH catalysts

Figure S1. The photograph of L-CoOOH weighed by an electronic balance. The screen shows that the mass of L-CoOOH is about 5.7 mg, which is obtained by LAL for 1 h.

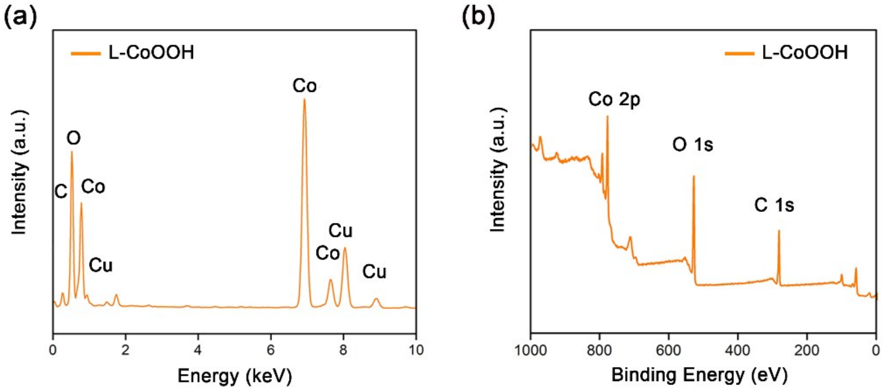

Figure S2. (a) EDS and (b) XPS spectra of L-CoOOH.

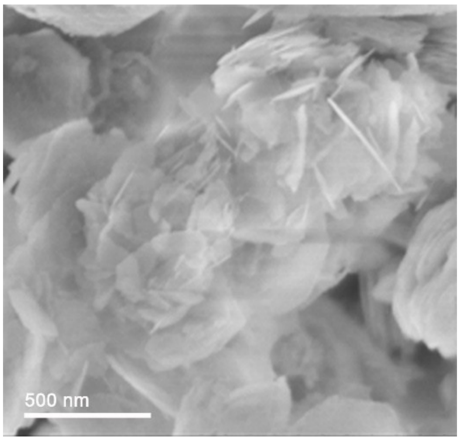

Figure S3. SEM image of L-CoOOH nanosheets.

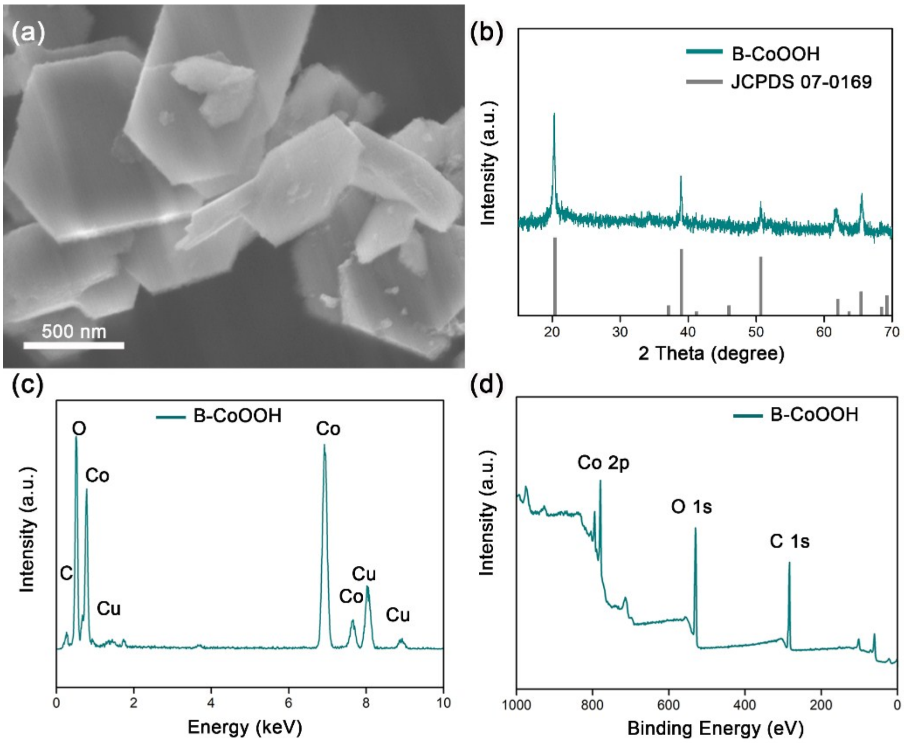

Figure S4. (a) SEM image and (b) XRD pattern of B-CoOOH. (c) EDS and (d) XPS spectra of B-CoOOH.

2. *OER performance test device*

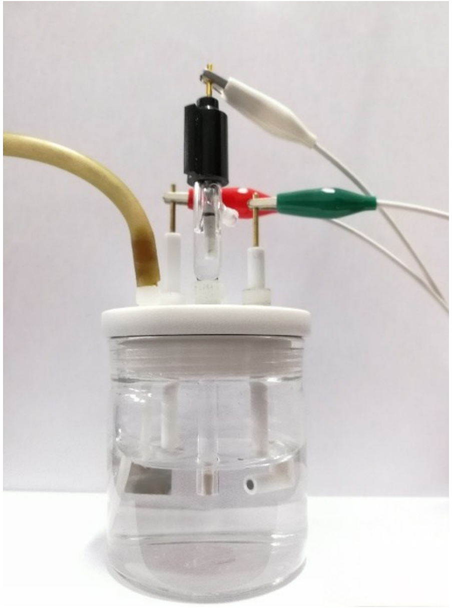

Figure S5. Experimental set-up of the three-electrode system for OER measurement in 1 M KOH solution. The platinum sheet and SCE electrode work as the counter and reference electrodes, respectively. The working electrode was prepared by depositing catalysts on the GCE.

3. *Electrochemical performances of Co-based catalysts*

Table S1. OER performances of L-CoOOH, B-CoOOH, and the reported Co-based catalysts in 1 M KOH solution.

Catalyst	Loading (mg cm^{-2})	$\eta_{10\ \mathrm{mA\ cm\text{-}2}}$ (mV)	Tafel slope (mV dec^{-1})	Ref
L-CoOOH	0.2	330	63.2	This work
B-CoOOH	0.2	410	75.4	This work
CoS_2 NPs	~1	430	81.4	[2]
$CoSe_2$ NPs	~1	424	78.3	[2]
CoOOH/G	0.2	401	47	[3]
Fe-CoOOH/G	0.2	330	37	[3]
C@Co-G	1	410	98.8	[4]
CoP/rGO-400	0.28	340	66	[5]
amorphous Co_2B	0.21	380	45	[6]
Co_3O_4 with vacancies	0.3	294	74	[7]
$Fe_{0.33}Co_{0.67}OOH$ PNSAs/CFC	1.39	266	30	[8]
$Zn_{0.45}Co_{2.55}O_4$	--	330	39	[9]
gamma-CoOOH	0.15	300	38	[10]
Fe/O doped Co_2P	2.187	274.5	51.7	[11]

NPs = Nanoparticles; G = Graphene; rGO = Reduced Graphene Oxide.

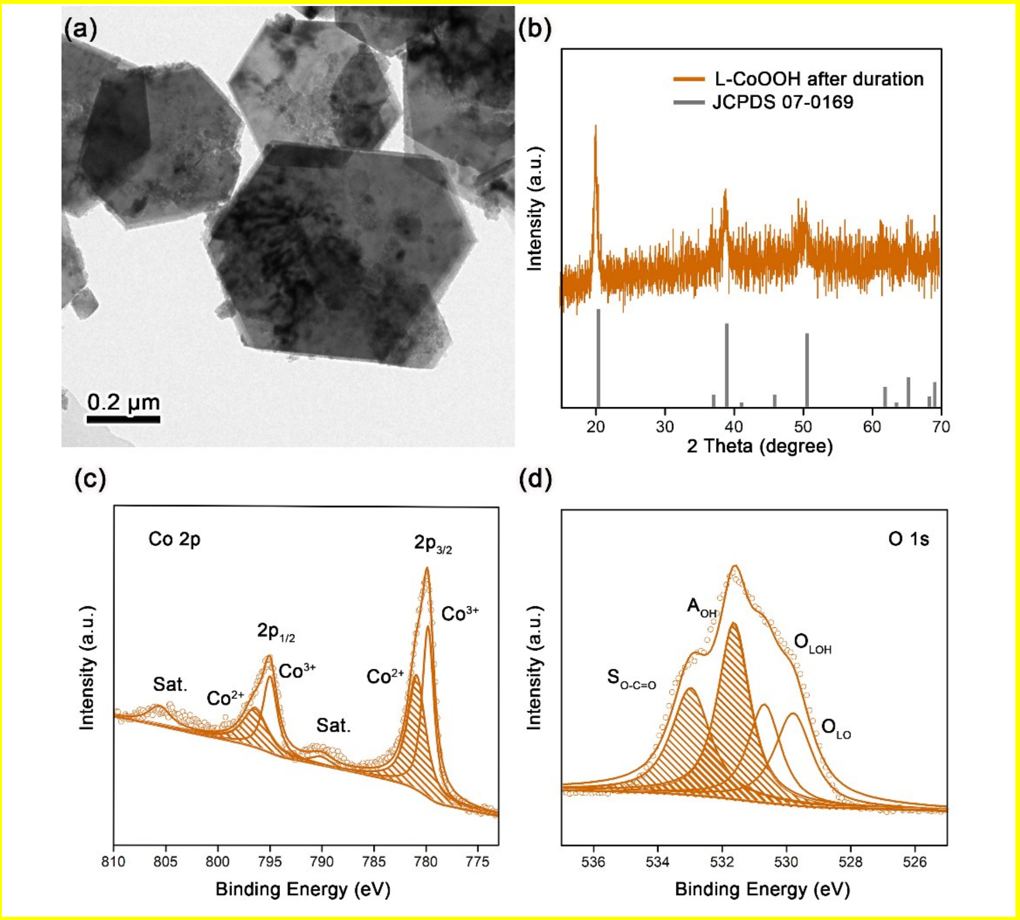

Figure S6. (a) Low-magnification TEM image and (b) XRD pattern of L-CoOOH after OER durability test. (c) Co 2p and (d) O 1s XPS spectra of L-CoOOH after OER durability test.

4. Analysis of the excellent OER activity of L-CoOOH

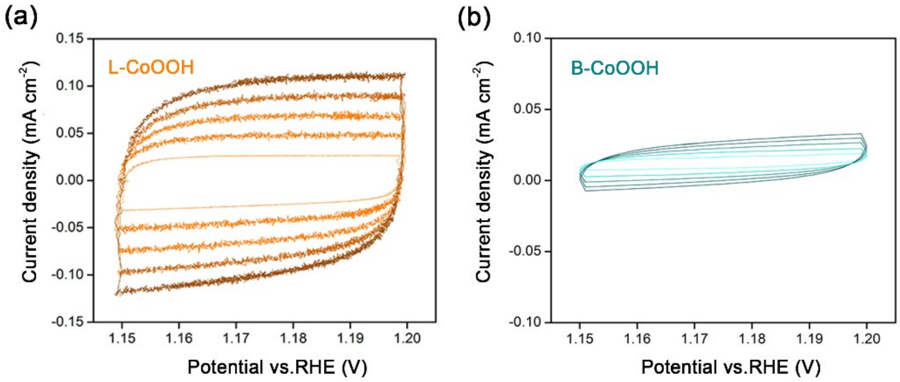

Figure S7. Electrochemical cyclic voltammetry (CV) curves of (a) L-CoOOH and (b) B-CoOOH. The selected potential range where no faradic current was observed is 1.15-1.20 vs. RHE, and the scan rates are 2, 4, 6, 8 and 10 mV s^{-1}.

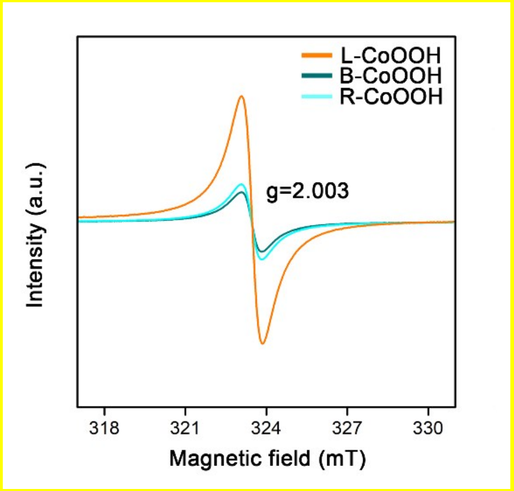

Figure S8. EPR spectra of L-CoOOH, B-CoOOH, and R-CoOOH.

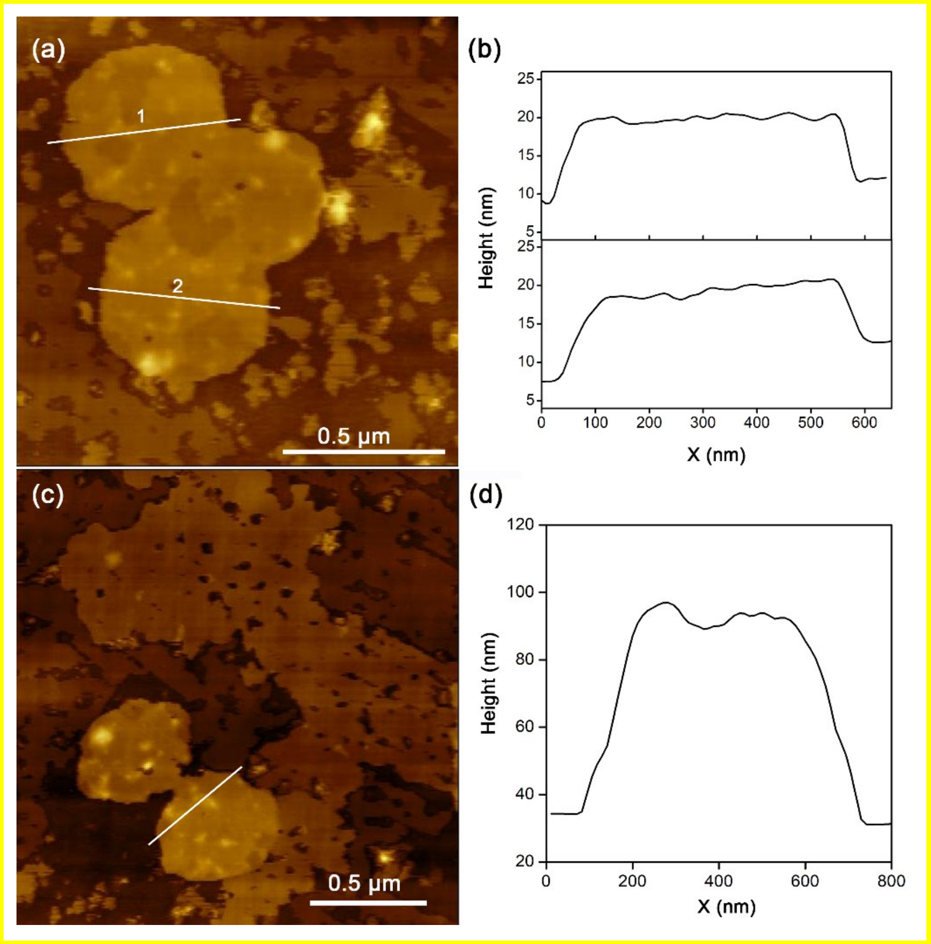

Figure S9. (a) AFM image and (b) height profiles of an individual L-CoOOH nanosheet. (c) AFM image and (d) height profile of an individual B-CoOOH nanosheet.

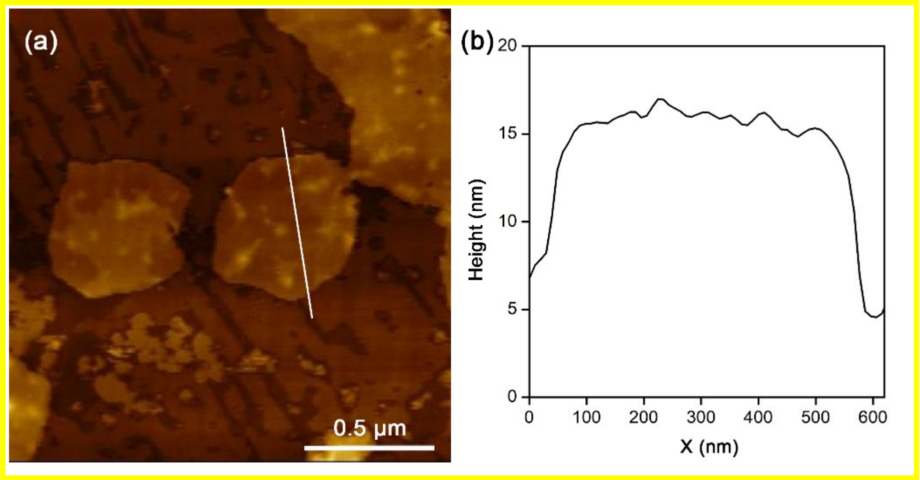

Figure S10. (a) AFM image and (b) height profile of a single R-CoOOH nanosheet.

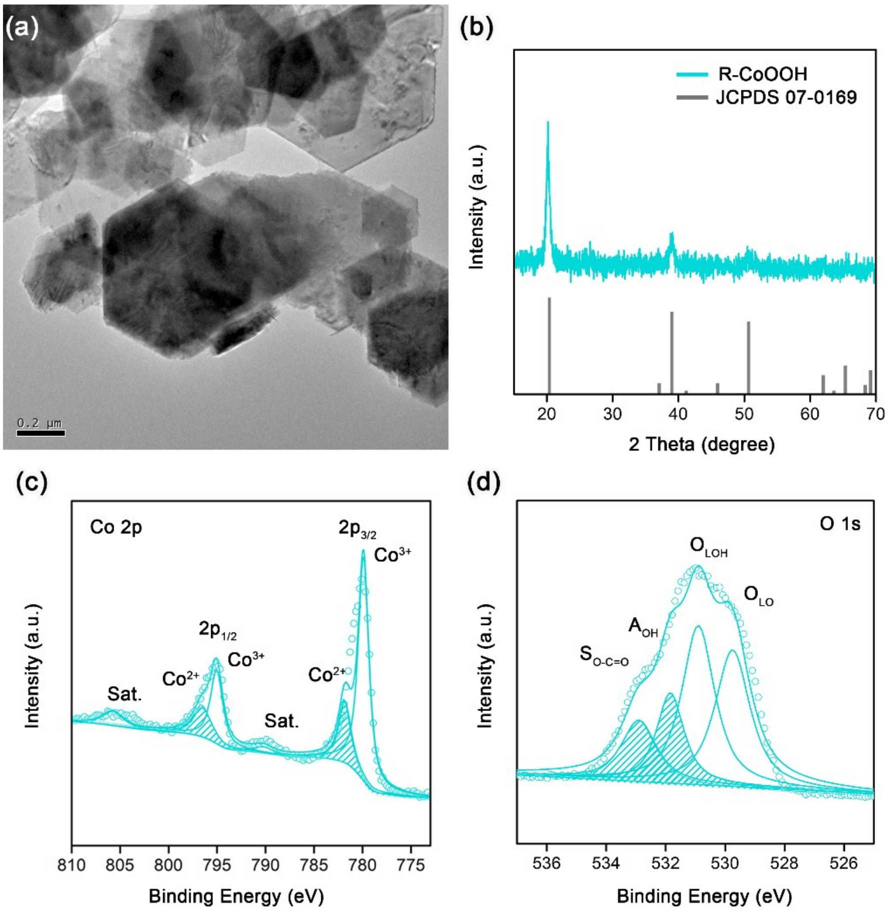

Figure S11. (a) Low-magnification TEM image and (b) XRD pattern of R-CoOOH. (c) Co 2p and (d) O 1s XPS spectra of R-CoOOH.

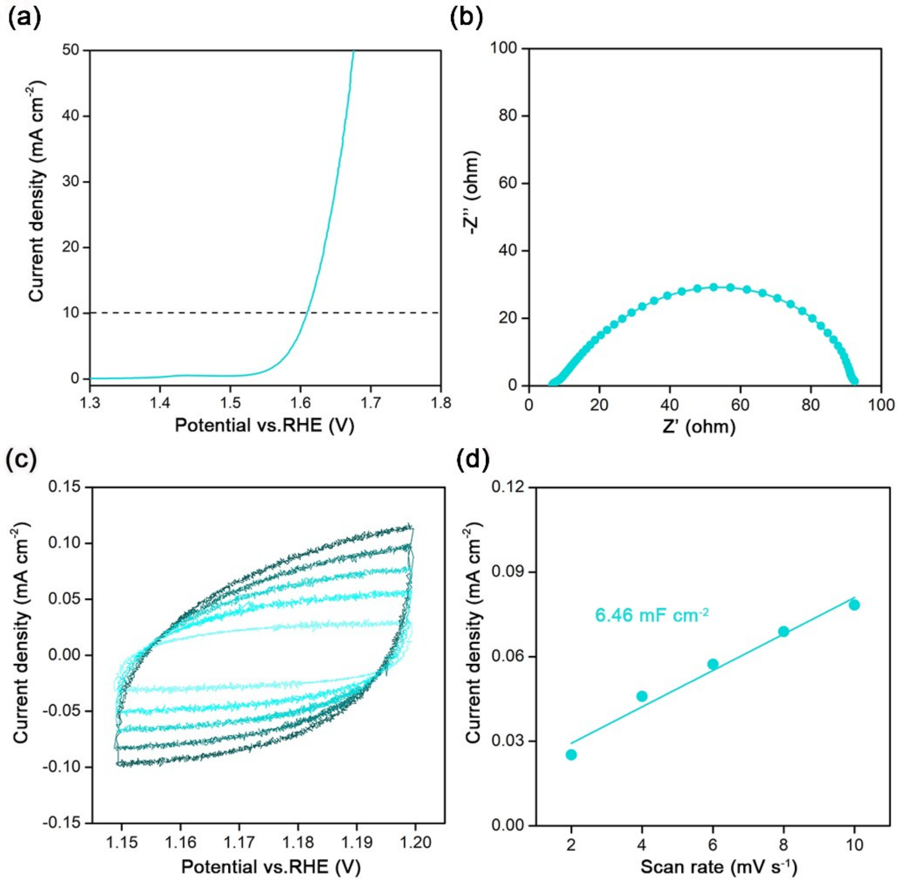

Figure S12. (a) LSV curve of R-CoOOH recorded in 1 M KOH with *iR*-correction. (b) The EIS of R-CoOOH recorded at the potential of 1.56 V_{RHE}. (c) Electrochemical CV curves of R-CoOOH. The selected potential range where no faradic current was observed is 1.15-1.20 vs. RHE, and the scan rates are 2, 4, 6, 8 and 10 mV s^{-1}. (d) The relationship between the current density and the scan rate.

Table S2. The impedance parameters derived by fitting the EIS responses.

Sample	R_s (Ω)	R_{ct} (Ω)
L-CoOOH	8.2	48.2
B-CoOOH	10.7	98.6
R-CoOOH	7.3	91.2

Table S3. Calculation of area percentages of different oxygen species obtained from the deconvoluted spectra.

	% area (O 1s)			
	lattice O	lattice OH	adsorbed OH	surface O-C=O
L-CoOOH	23.8 %	16.5 %	34.7 %	25.0 %
B-CoOOH	38.1 %	32.6 %	18.6 %	10.7 %
R-CoOOH	32.6 %	35.8 %	16.9 %	14.7 %

5. *Computational details*

All the DFT calculations were performed using the Vienna Ab-initio Simulation Package (VASP),[12, 13] employing the Projected Augmented Wave[14] (PAW) method. The Perdew-Burke-Ernzerhof (PBE) functional was used to describe the exchange and correlation effect.[15] For all the geometry optimizations, the cutoff energy was set to be 450 eV. The 9×9×2 Monkhorst-Pack grids[16] were set to optimize the bulk structure of CoOOH. The (012) facet was used to represent the catalytic surface of CoOOH. Reciprocally proportional to the lattice parameters, a 4×3×1 and 10×6×1 mesh were used to perform the calculations of surface adsorption and density of states, respectively. At least 15 Å vacuum layer was applied in z-direction of the slab models, preventing the vertical interactions between slabs.

In aqueous conditions, OER could occur in the following four elementary steps:

$$\text{Step I}: OH^- + * \rightarrow *OH + e^- \qquad \text{(S1)}$$

$$\text{Step II}: *OH + OH^- \rightarrow *O + H_2O + e^- \qquad \text{(S2)}$$

$$\text{Step III}: *O + OH^- \rightarrow *OOH + e^- \qquad \text{(S3)}$$

$$\text{Step IV}: *OOH + OH^- \rightarrow * + O_2 + H_2O + e^- \qquad \text{(S4)}$$

where * denotes the active sites on the catalyst surface. Based on the above mechanism, the free energy of three intermediate states, *OH, *O, and *OOH, are important to identify a given material's OER activity. The computational hydrogen electrode (CHE) model[17] was used to calculate the free energies of OER, based on which the free energy of an adsorbed species is defined as

$$\Delta G_{ads} = \Delta E_{ads} + \Delta E_{ZPE} - T\Delta S_{ads} \qquad \text{(S5)}$$

where ΔE_{ads} is the electronic adsorption energy, ΔE_{ZPE} is the zero point energy difference between adsorbed and gaseous species, and $T\Delta S_{ads}$ is the corresponding entropy difference between these two states. The electronic binding energy is referenced as ½ H_2 for each H atom, and (H_2O – H_2) for each O atom, plus the energy of the clean slab. The corrections of zero point energy and entropy of the OER intermediates can be found in Table S4.

Table S4. The correction of zero point energy and entropy of the adsorbed and gaseous species.

	ZPE (eV)	TS (eV)
*OOH	0.35	0
*O	0.05	0
*OH	0.31	0.01
H_2O	0.56	0.67
H_2	0.27	0.41

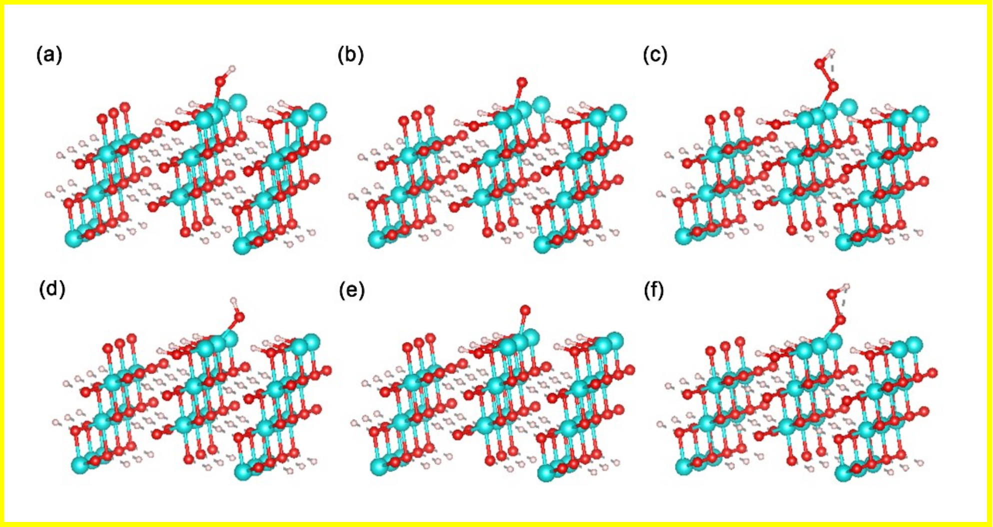

Figure S13. Optimized structures after adsorption of *OH, *O and *OOH intermediates on (a-c) CoOOH with perfect surface and (d-f) CoOOH with oxygen vacancies. Color code: white for H, red for O, and cyan for Co.

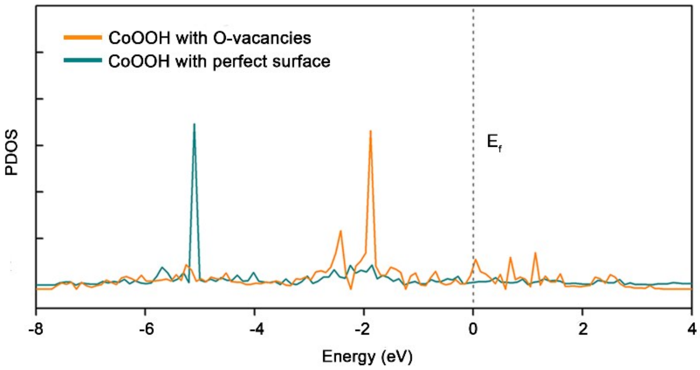

Figure S14. The PDOS on CoOOH with perfect surface and CoOOH with oxygen vacancies.

Supplementary References

1. Y. Z. Xu, C. Z. Yuan and X. P. Chen, *Appl. Surf. Sci.*, 2017, **426**, 688-693.
2. L. Fang, W. Li, Y. Guan, Y. Feng, H. Zhang, S. Wang and Y. Wang, *Adv. Funct. Mater.*, 2017, **27**, 1701008.
3. X. Han, C. Yu, S. Zhou, C. Zhao, H. Huang, J. Yang, Z. Liu, J. Zhao and J. Qiu, *Adv. Energy. Mater.*, 2017, **7**, 1602148.
4. W. Yang, L. Chen, X. Liu, J. Jia and S. Guo, *Nanoscale*, 2017, **9**, 1738-1744.
5. L. Jiao, Y. X. Zhou and H. L. Jiang, *Chem. Sci.*, 2016, **7**, 1690-1695.
6. J. Masa, P. Weide, D. Peeters, I. Sinev, W. Xia, Z. Sun, C. Somsen, M. Muhler and W. Schuhmann, *Adv. Energy. Mater.*, 2016, **6**, 1502313.
7. Y. Zhou, C. K. Dong, L. L. Han, J. Yang and X. W. Du, *ACS Catal.*, 2016, **6**, 6699-6703.
8. S. H. Ye, Z. X. Shi, J. X. Feng, Y. X. Tong and G. R. Li, *Angew. Chem.*, 2018, **57**, 2672-2676.
9. S. Han, S. Liu, R. Wang, X. Liu, L. Bai and Z. He, *ACS Appl Mater Inter*, 2017, **9**, 17186-17194.
10. J. Huang, J. Chen, T. Yao, J. He, S. Jiang, Z. Sun, Q. Liu, W. Cheng, F. Hu, Y. Jiang, Z. Pan and S. Wei, *Angew. Chem.*, 2015, **54**, 8722-8727.
11. J. Duan, S. Chen, A. Vasileff and S. Z. Qiao, *ACS Nano*, 2016, **10**, 8738-8745.
12. G. Kresse and J. Furthmüller, *Phys. Rev. B.*, 1996, **54**, 11169-11186.
13. G. Kresse and J. Hafner, *Phys. Rev. B.*, 1994, **49**, 14251-14269.
14. P. E. Blöchl, *Phys. Rev. B.*, 1994, **50**, 17953-17979.
15. J. P. Perdew, K. Burke and M. Ernzerhof, *Phys. Rev. Lett.*, 1996, **77**, 3865-3868.
16. H. J. Monkhorst and J. D. Pack, *Phys. Rev. B.*, 1976, **13**, 5188.
17. J. K. Nørskov, J. Rossmeisl, A. Logadottir, L. Lindqvist, J. R. Kitchin, T. Bligaard and H. Jonsson, *J Phys Chem B*, 2004, **108**, 17886-17892.